EXAMINATION OF NEAR-WALL SCALING FOR TURBULENT BOUNDARY LAYERS WITH ADVERSE PRESSURE GRADIENT

Nikolaus Peller, Michael Manhart
Fachgebiet Hydromechanik,
Technische Universität München
Arcisstrasse 21, D-80333 München, Germany
n.peller@bv.tum.de, m.manhart@bv.tum.de

Margareta Petrovan Boiarciuc
Polytech'Orléans/LME,
8 rue Léonard de Vinci, 45072 Orleans CEDEX 2, France,
margareta-elena.boiarciuc@univ-orleans.fr

Christophe Brun
Laboratoire d'Etudes Géophysiques et Industrielles/MoST,
BP 53, 38041 Grenoble CEDEX 9, France,
christophe.brun@hmg.inpg.fr

ABSTRACT

Based on earlier work in Peller et al. (2005) and Manhart et al. (2006) we further investigate the behaviour of an extended scaling for turbulent flows including a streamwise pressure gradient. The scaling is based on a combination of the friction velocity U_τ and the pressure velocity U_p leading to a combined velocity scale $U_{\tau p}$. The influence of pressure gradient with respect to wall friction is quantified by a non-dimensional parameter $\alpha = U_\tau / U_{\tau p} \in [0, 1]$. We investigate Reynolds, convective and pressure terms within the streamwise momentum balance as well as the viscous and turbulent stresses, based on DNS of two types of separated flows. We find good agreement in the profiles when they are ploted in extended wall normal coordinates for positions characterized by a similar α value. In most cases we can confirm the assumption of a constant streamwise pressure gradient in wall normal direction, except when curvature effects are present, which modifies the pressure gradient distribution. For a given α we observe universal behaviour for the velocity profiles that shows very good agreement over a complete recirculation region. Accordingly, the terms in the momentum balances agree well and this gives hope to describe universal behaviour of e.g. Reynolds terms depending on the parameter α.

INTRODUCTION

Several studies (Stratford (1959); Simpson (1989)) have addressed the near-wall behaviour of turbulent flows when pressure gradient effects are present. In order to find universal velocitiy profiles even in such cases a scaling is the key issue. In zero pressure gradient flows the proper scaling is based on the wall friction and leads to the well known law of the wall. Very often, for situations with increasing pressure gradient this scaling ist still applied. But, for situations where the flow separates it is not applicable any more since the wall friction yields zero. On the other hand e.g. Skote et al. (2000) apply a scaling based on the pressure gradient for the separation point. The question arises what scaling should be used in the region where both effects are present. Peller et al. (2005) and Manhart et al. (2006) have addressed this issue and proposed a scaling based on both, pressure gradient and wall friction which allows a smooth transition between regions dominated by friction and regions dominated by pressure gradient. A universal behaviour of velocity profiles has been investigated under the proposed scaling for the viscous region. In the present work, we concentrate on the universality of terms in the momentum balance normalized by the extended scaling. The results show that there is a universal behaviour within limits of e.g. Reynolds and convective terms which gives hope for modeling approaches.

TEST CASES

We investigate two different types of separated flows, a turbulent boundary layer along a flat plate (BL) (Manhart and Friedrich (2002)) and the flow over a periodic arrangement of two-dimensional hills (PH) (Peller and Manhart (2006)). All flows have been computed by means of Direct Numerical Simulation (DNS). The numerical scheme used for the simulations is based on a Finite Volume solver on a non-equidistant Cartesian grid (Peller et al. (2006)).

Separating turbulent boundary layer along a flat plate (BL)

The turbulent boundary layer simulation is designed according to an experiment performed by Kalter and Fernholz (1994). In this experiment, a turbulent boundary layer developing along a circular cylinder is subjected to a streamwise adverse pressure gradient until separation occurs. In comparison to the experiment the Reynolds number has been lowered to $Re_\theta = 870$ (based on inlet free-stream velocity and inlet momentum thickness) because of computational expenses. The simulation has been performed in a rectangular domain selected in a way to cover the separation bubble (see Figure 1).

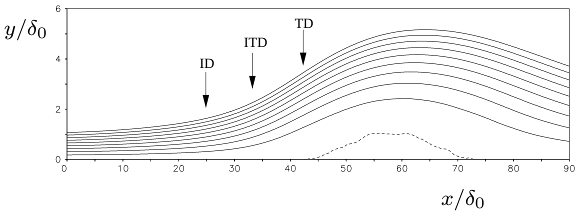

Figure 1: Streamlines for BL case.

Based on wall shear stress of the oncoming boundary layer, the grid spacings were $\Delta x^+ = 11.7$, $\Delta y^+ = 1.6$ and $\Delta z^+ = 7.2$ in streamwise, wall normal and spanwise direction, respectively. It was shown in a grid study and by comparison with the experiment of Kalter and Fernholz (1994) that the resolution and the size of the computational domain were sufficient to get a highly accurate data base of this flow. We used a fully turbulent inflow condition, generated by fluctuations taken from a downstream position which are superposed to a time averaged boundary layer profile corresponding to the desired boundary layer thickness and Reynolds number. In spanwise direction, we used periodic conditions, at the outflow a zero-gradient for the velocities. The bottom wall is described by a no-slip condition and at the top, the desired pressure profile is prescribed in combination with a zero gradient for the velocities.

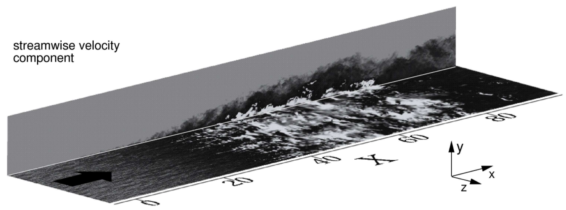

Figure 2: Instantaneous streamwise velocity component at the wall and in a streamwise/wall-normal plane.

The separation of the boundary layer ($Re_\theta = 870$) is driven by an adverse pressure gradient which is adjusted to yield a marginal separation with a maximal backflow coefficient of 70%. The separation bubble starts at $x/\delta_o = 44$ and is thin compared to the inlet boundary layer thickness. The dynamics in the separation zone are strongly affected by large scale structures reaching from the shear layer above the separation bubble to the wall. Figure 2 gives an idea of the complexity of the instantaneous flow. The separation line is not fixed, but strongly fluctuates in space and time. The labels in Figure 1 mark the regions of incipient detachment (ID, 1% backflow), intermittent transitory detachment (ITD, 20% backflow) and transitory detachment (TD, 50% backflow) according to the definitions of Simpson (1989). TD is at the same position as $\tau_w = 0.0$. The point of incipient detachment is identifiable with the first occurrence of these strong large scale structures. According to Simpson, this is also the point at which the mean velocity profile starts to deviate from the logarithmic law of the wall. From this point on, one would expect that standard wall models based on the law of the wall start to fail. From $x/\delta_0 = 34$ (ITD) on both, linear and logarithmic laws start to fail.

Channel flow with constrictions (PH)

Our second test case is the turbulent flow in a channel with periodically arranged hills at the bottom wall. The numerical setup was introduced by Mellen et al. (2000). A detailed investigation of this flow at $Re = 10595$ has been undertaken by Fröehlich et al. (2005) on the basis of a LES. Based on hill height h, the channel extends $9.0h$ in streamwise, $4.5h$ in spanwise and $3.035h$ in wall-normal direction. The hills are arranged at the distance $9.0h$. The Reynolds number based on the bulk velocity and the hill height is $Re = 5600$. In streamwise and spanwise direction periodic boundary conditions are used. On the hill surface a no-slip condition is applied as well as on the top of the channel wall.

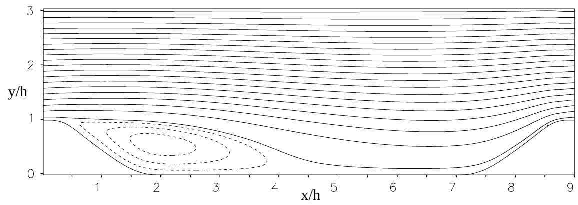

Figure 3: Streamlines for PH case.

The configuration can be seen in Figure 3 which shows streamlines of the average velocity. The flow separates at the hill crest at $x/h = 0.17$ and forms a large separation bubble reaching to $x/h = 5.0$. The separation in this case is not only due to an adverse pressure gradient but also the result of the strong streamwise curvature of the lower wall. Thus it establishes a completely different test bed than the flat plate boundary layer for our investigations. The computational grid has $233 \cdot 10^6$ grid cells. The resulting near-wall grid spacings based on maximum wall shear stress are $\Delta x^+ = 8$, $\Delta y^+ = 6.3$ and $\Delta z^+ = 1.2$ in streamwise, spanwise and wall normal direction, respectively. A considerable negative wall shear stress exists at $x/h \approx 3.0$ within the recirculation bubble which shows that a strong backflow develops in the recirculation zone. A second tiny recirculation zone is present at $x/h \approx 7.2$ just before the hill. On the windward side of the hill, a sharp peak of wall shear stress evolves that is the result of the strong acceleration of the flow due to the convergence of the channel in this region. This acceleration is driven by a pressure drop, i.e. a negative streamwise pressure gradient.

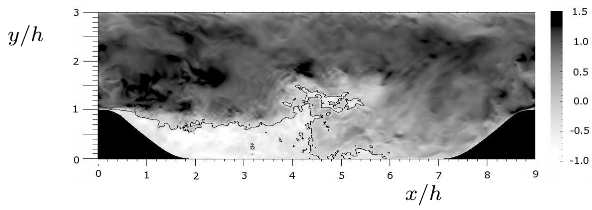

Figure 4: Flow over a periodic arrangement of hills: instantaneous streamwise velocity component. The black line indicates $u = 0$.

Shortly after the main separation, the roll-up process in the shear layer bounding the separation zone leads to large scale fluctuations of high turbulence intensity (Figure 4). Nevertheless, there is a relatively calm region in the separation bubble. The fluctuations of the separation line are comparably smaller than in the flat plate case, since it is also determined by the point of maximum curvature at the hill crest. The reattachment line however fluctuates strongly and instants in time occur, during which the whole bottom wall shows reverse flow.

EXTENDED INNER SCALING

We analyse the near-wall behaviour of time-averaged flow fields in the proximity of a wall under the influence of a streamwise pressure gradient. The behaviour of velocity profiles in the viscous region has been documented in Manhart et al. (2006) and Peller et al. (2005). Certain assumptions have to be made to describe the profiles analytically. We will give a brief review in the following. Starting from the streamwise momentum balance in its differential form we integrate and derive the extended law of the wall. Hereby we concentrate on the effect of the terms in the momentum balances in integrated and differential form. The classical law-of-the wall e.g. separates the near-wall region into a viscous zone, in which only viscous forces play a role and a turbulent zone in which viscous forces are negligible. We are interested in the behaviour of viscous forces, convective and Reynolds terms in zones where the pressure gradient is not zero.

Momentum balances

We consider time averaged velocity profiles in two-dimensional flows for which the mean streamwise momentum balance comprises contributions of convection ($C1$), pressure gradient ($P1$), diffusion ($D1$) and Reynolds stresses ($R1$) :

$$0 = \underbrace{-\left(\frac{\partial UU}{\partial x} + \frac{\partial UV}{\partial y}\right)}_{C1} \underbrace{-\frac{1}{\rho}\frac{\partial P}{\partial x}}_{P1} \underbrace{+\nu\left(\frac{\partial^2 U}{\partial x^2} + \frac{\partial^2 U}{\partial y^2}\right)}_{D1} \underbrace{-\left(\frac{\partial \overline{u'u'}}{\partial x} + \frac{\partial \overline{u'v'}}{\partial y}\right)}_{R1} \quad (1)$$

Multiplying equation (1) by ρ and integrating in wall-normal direction leads to the balance of Pressure force ($P2$), viscous stress ($D2$), total stress (τ_t) and wall friction (τ_w):

$$0 = \underbrace{-\int_o^y \frac{\partial P}{\partial x} dy}_{P2} \underbrace{+\mu\frac{\partial U}{\partial y}}_{D2} + \tau_t - \tau_w \quad (2)$$

We follow Kaltenbach (2003) and subsume the convective ($C2$) term, Reynolds stresses ($R2$) and the viscous stresses ($D2$) in streamwise direction into a total stress τ_t:

$$\tau_t = \underbrace{-\left(\int_0^y \rho\frac{\partial UU}{\partial x} dy + \rho UV\right)}_{C2} \underbrace{+\int_0^y \mu\frac{\partial^2 U}{\partial x^2} dy}_{RES} \underbrace{-\left(\int_0^y \rho\frac{\partial \overline{u'u'}}{\partial x} dy + \rho\overline{u'v'}\right)}_{R2} \quad (3)$$

The main issue related to these balances is the relative importance of each term and the range where they can be neglected. In addition to this the question arises if universality can be found for separate terms or their respective sums under a certain scaling. We will use the scaling introduced in Peller et al. (2005) and Manhart et al. (2006) as described in the following section.

Extended inner scaling

We introduce a proper scaling, i.e. proper velocity, length and time scales to non-dimensionalise the momentum equation. Since we seek these reference values for the near-wall region, we refer to them as inner scales:

$$u_\tau = \left|\frac{\tau_w}{\rho}\right|^{1/2}, \qquad u_p = \left|\frac{\mu}{\rho^2}\frac{\partial P}{\partial x}\right|^{1/3}, \qquad u_{\tau p} = \sqrt{u_\tau^2 + u_p^2} \quad (4)$$

The standard reference velocity for inner scaling is the friction velocity u_τ. Following Skote et al. (2000), we define an additional velocity scale u_p, which is based on the streamwise pressure gradient. The combined scale $u_{\tau p}$ takes both into account. We refer to this velocity scale as extended inner velocity scale or extended inner scaling, alternatively. Based on the extended inner velocity scale $u_{\tau p}$, the non-dimensional velocity u^* and length y^* are defined by:

$$U^* = \frac{U}{u_{\tau p}} \qquad y^* = \frac{y u_{\tau p}}{\nu} \quad (5)$$

With these reference values, the velocity profile in the viscous region including pressure gradient effects writes in non-dimensional form as a function of only two non-dimensional parameters $U^* = f(y^*, \alpha)$ of which $\alpha \in [0, 1]$ quantifies the relative importance of each of the two involved velocity scales. The ratio between classical $(u^+; y^+)$ and extended inner coordinates $(u^*; y^*)$ can also be expressed in terms of α.

$$\alpha = \frac{u_\tau^2}{u_\tau^2 + u_p^2} = \frac{u_\tau^2}{u_{\tau p}^2}, \qquad \frac{u^*}{u^+} = \sqrt{\alpha}, \qquad \frac{y^*}{y^+} = \frac{1}{\sqrt{\alpha}} \quad (6)$$

Normalisation and extended law of the wall

The momentum balance in equation (1) is normalised by $u_{\tau p}^3/\nu$ and the integrated momentum balance in equation (2) is normalised by $\rho u_{\tau p}^2$. Integrating once more we end up with an expression for the streamwise velocity profile. Under standard boundary layer assumptions this equation leads to the linear law of the wall within the viscous region. When the pressure gradient cannot be neglected we obtain the extended law of the wall:

$$U^*(y^*) = sign(\tau_w)\alpha y^* + sign\left(\frac{\partial P}{\partial x}\right)\frac{1}{2}(1-\alpha)^{3/2} y^{*2} \quad (7)$$

The signs of the pressure gradient and wall friction are necessary to define the direction of the flow and the direction of the pressure term, in complement to the amplitude of α. The range of validity of equation (7) is of high importance for the construction of explicit wall models. It has to be defined in terms of the dimensionless wall distance y^* and will certainly be a function of α. The range of validity will strongly depend on how fast the Reynolds terms and the convective terms gain weight in the momentum balance, when moving away from the wall. If, however the increase of the Reynolds terms with respect to wall distance follows a universal form (determined by wall conditions), then we would observe a universal behavior of the velocity profiles even when equation (7) is no longer valid.

The classical law of the wall $U^+ = y^+$ can be written in terms of the extended inner coordinates: $U^* = \alpha y^*$ It has to be noted that in case of vanishing streamwise pressure gradient ($\alpha = 1.0$), the classical law of the wall for the viscous region $U^* = y^*$ (or alternatively: $U^+ = y^+$) is recovered. It is generally accepted, that this equation is valid below $y^+ = 5$. When the wall shear stress is zero the quadratic velocity profile, $U^* = \frac{1}{2}y^{*2}$, is obtained in the viscous region. For realistic flow configurations, both contributions are blended in equation (7).

ANALYSIS OF THE FLOW DYNAMICS

We now turn to the near-wall behaviour of the terms in the momentum balance and the behaviour of the velocity profiles up to the turbulent regime. In what follows, we investigate (i) the momentum balance, (ii) the stresses and (iii) the velocity profiles , all normalized by the extended scaling. For this, we select positions in the flow cases in which specific values of α are obtained. In a classical attached turbulent boundary layer α would be one. Here, we restrict ourselves to two α values, namely $\alpha \approx 0.6$ and $\alpha \approx 0.0$. In the more general case of $\alpha \approx 0.6$ both, wall friction and pressure gradient effects are present. For $\alpha = 0$ it is either a point of separation or of reattachment. For $\alpha \neq 0$ one has to take care of the signs of the wall shear stress and the streamwise pressure gradient. When both have the same sign, their action on the velocity profile is in the same direction. When they have opposite signs, they act in opposite direction and it can be possible that the flow changes direction. Therefore, we distinguish between these two situations.

General situation ($\alpha \approx 0.6$)

For the situation $\alpha \approx 0.6$, we selected three profiles for the case when shear stress and pressure gradient act in the same direction and three for the other, in total four profiles from (BL) and two from (PH). In Figure 5 terms of the momentum balance (equation 1) are plotted: viscous term ($D1$), pressure term ($P1$) and the sum of Reynolds and convective terms ($R1 + C1$). The profiles are plotted on top of each other in extended inner coordinates.

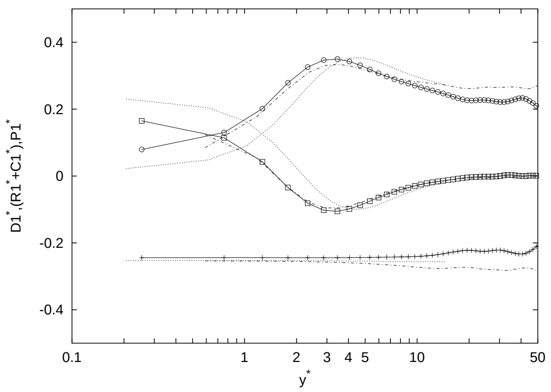

Figure 5: Momentum balance in extended inner coordinates for $\alpha \approx 0.6$. $(\tau_w) \cdot (\partial P/\partial x) > 0$. ——— BL at $x/\delta_0 = 36.5$; $-\cdot-\cdot-$ BL at $x/\delta_0 = 77$; $\cdot\cdot\cdot\cdot\cdot\cdot$ PH at $x/h = 5.6$; $\square$ viscous term D1; $\bigcirc$ Reynolds and convective term (R1+C1); $+$ pressure term P1;

One can observe that the assumption of a constant pressure gradient is valid in good approximation up to a wall distance of $y^* = 50$. By normalisation the pressure gradient yields the value $-(1-\alpha)^{(3/2)} = -0.25$ at the wall. The absolute value of the viscous term is equal to the pressure term at the wall since the Reynolds terms go to zero. The most important observation is that despite deviations close to the wall the Reynolds and diffusive terms of all cases have similar slopes and reach the same maximum amplitude. The Reynolds terms reach the maximum at about $y^* = 4$. After the maximum they lie on top of each other.

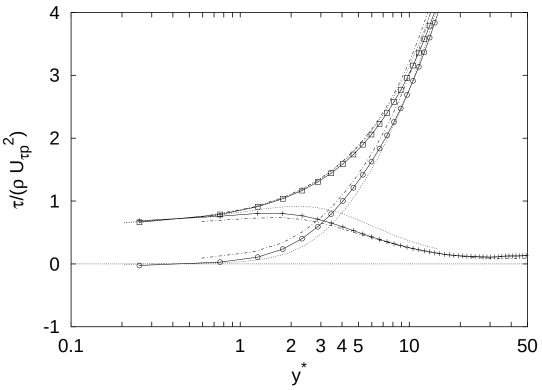

Figure 6: Balance of stresses in extended inner coordinates for $\alpha \approx 0.6$. $(\tau_w) \cdot (\partial P/\partial x) > 0$. ——— BL at $x/\delta_0 = 36.5$; $-\cdot-\cdot-$ BL at $x/\delta_0 = 77$; $\cdot\cdot\cdot\cdot\cdot\cdot$ PH at $x/h = 5.6$; $\square$ pressure term and wall stress $(P2 + \tau_w)$; $\bigcirc$ total stress τ_t; $+$ viscous term D2;

By integration we have obtained equations (2), (3). In Figure 7 we plot from this equation the sum of the pressure term and the wall shear stress $(P2 + \tau_w)$, the viscous term $(D2)$ and the remaining total shear stress (τ_t). The pressure term P2 is zero at the wall and the sum $(P2 + \tau_w)$ yields τ_w which is equal to $\alpha = 0.6$ if normalized by the exended scaling. For better visualization the sign of $(P2 + \tau_w)$ is inverted. This way the sum of the viscous term plus total shear stress must equal the term $(P2 + \tau_w)$. Again we can see that differences in the viscous term are reflected in the Reynolds term. But the pressure term is identical in all cases. Also, the limit of the viscous term is identical.

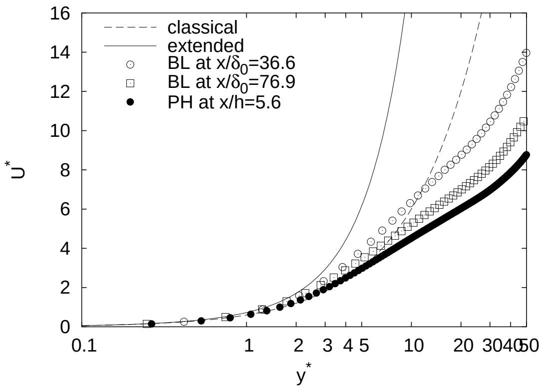

Figure 7: Velocity profiles in extended inner coordinates for $\alpha \approx 0.6$. $(\tau_w) \cdot (\partial P/\partial x) > 0$.

From the velocity profile (Figure 7) we can see the result from integrating the diffusive term ($D2$) in Figure 6. The profiles agree well with the extended law of the wall (equation 7) until $y^* = 2$ and start to deviate from there which is a result of the Reynolds terms below $y^* = 2$. Later on the slope of the profiles remains similar to each other which is due to the convergence of Reynolds and diffusive terms observed in the momentum balances (Figure 5 and 6).

Now we turn to the situation where wall friction and pressure gradient have opposite signs. The terms of the momentum balance are plotted in Figure 8. The agreement among different cases is even better than in the latter case where pressure gradient and wall friction have the same sign. This time Reynolds terms and convective terms lie on top of each other. Only for the periodic hill (PH) case deviations in the pressure gradient can be observed. The assumption of a constant pressure gradient starts to fail at $Y^* = 10$. This is due to curvature effects, because the selected position is located at the beginning of the hill slope.

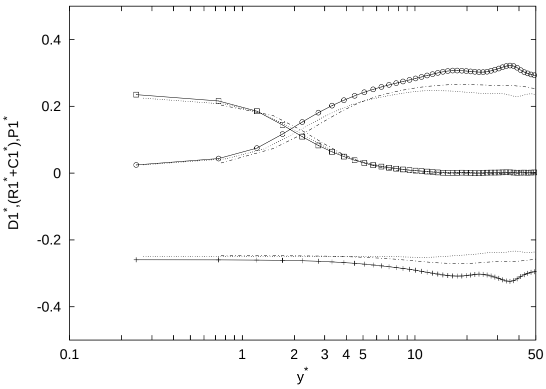

Figure 8: Momentum balance in extended inner coordinates for $\alpha \approx 0.6$. $(\tau_w) \cdot (\partial P/\partial x) < 0$. ——— BL at $x/\delta_0 = 50$; $- \cdot - \cdot -$ BL at $x/\delta_0 = 65$; $\cdot\ \cdot\ \cdot\ \cdot\ \cdot\ \cdot$ PH at $x/h = 4.3$; □ viscous term D1; ○ Reynolds and convective term (R1+C1); + pressure term P1;

The remarkable agreement is also observed in the integrated momentum balance, i.e. the stresses. This time the wall friction is negative and the sum of pressure term plus wall friction ($P2 + \tau_w$) must yield -0.6. Also the viscous term must yield this value. The deviation of the pressure gradient for the periodic hill case is not as obvious as in the momentum balance.

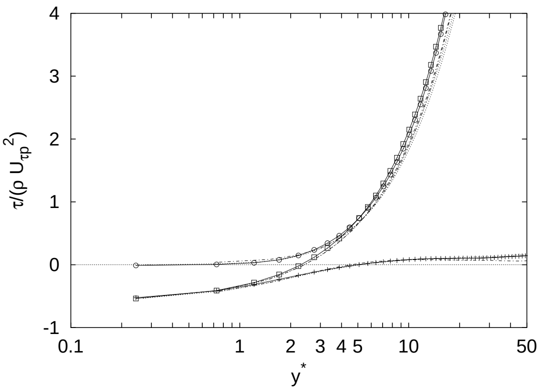

Figure 9: Balance of stresses in extended inner coordinates for $\alpha \approx 0.6$. $(\tau_w) \cdot (\partial P/\partial x) < 0$. ——— BL at $x/\delta_0 = 50$; $- \cdot - \cdot -$ BL at $x/\delta_0 = 65$; $\cdot\ \cdot\ \cdot\ \cdot\ \cdot\ \cdot$ PH at $x/h = 4.3$; □ pressure term and wall stress $(P2 + \tau_w)$; ○ total stress τ_t; + viscous term D2;

The good agreement for the velocity profile was to be expected from the observations in the momentum balance. But it is surprising that the profiles show a universal behaviour over the complete recirculation region. Even after the recirculation the profiles stay close to each other up to $y^* = 30$. After that the profile taken from (PH) deviates stronger than the other profiles. This can be contributed to the pressure gradient which is no longer constant in this region. Again, equation (7) describes the profiles well up to $y^* = 2$. After that the effects of Reynolds and convective terms becomes dominant.

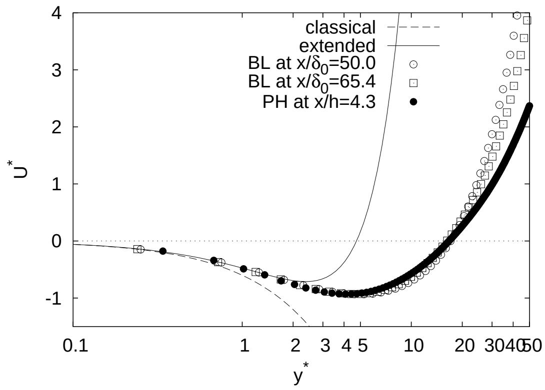

Figure 10: Velocity profiles in extended inner coordinates for $\alpha \approx 0.6$. $(\tau_w) \cdot (\partial P/\partial x) < 0$

Situations dominated by pressure gradient ($\alpha \approx 0$)

When the wall shear stress is zero ($\alpha \approx 0$), we do not have to distinguish between the two cases depending on the sign of pressure gradient. The wall friction is zero and the value of the pressure gradient in the non-dimensional momentum balance yields one. The limiting behaviour can be observed in Figure 11. As in the previous cases, differences among the cases can be mainly observed close to the wall. Apart from the wall all profiles behave similarly. As in the preceeding case the profile for the periodic hill (PH) shows a pressure gradient which does not remain constant over $y^* \approx 15$.

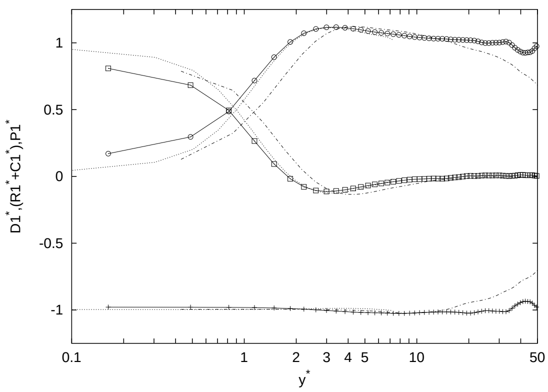

Figure 11: Momentum balance in extended inner coordinates for $\alpha \approx 0.0$. $\tau_w \approx 0$. ——— BL at $x/\delta_0 = 42$; $- \cdot - \cdot -$ BL at $x/\delta_0 = 73$; $\cdot\ \cdot\ \cdot\ \cdot\ \cdot\ \cdot$ PH at $x/h = 7$; □ viscous term D1; ○ Reynolds and convective term (R1+C1); + pressure term P1;

In the integrated momentum balance, i.e. the stresses, deviations can be seen for the periodic hill case similar to the momentum balance. The deviations in the slope of the Reynolds and viscous terms have already been observed in the momentum balance. The crossing of the viscous term and the Reynolds term in the differential momentum balance (11) is identical for the boundary layer profile but shifted in the periodic hill case. This is reflected in the crossing of viscous and total stresses.

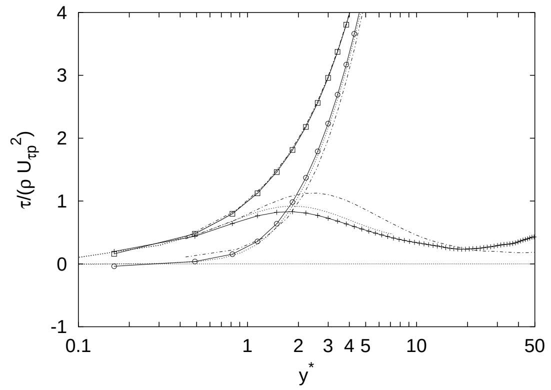

Figure 12: Balance of stresses in extended inner coordinates for $\alpha \approx 0.0$. $\tau_w \approx 0$. ——— BL at $x/\delta_0 = 42$; $-\cdot-\cdot-\cdot$ BL at $x/\delta_0 = 73$; $\cdot\cdot\cdot\cdot\cdot\cdot$ PH at $x/h = 7$; □ pressure term and wall stress $(P2 + \tau_w)$; ○ total stress τ_t; + viscous term D2;

Starting from the observations with the momentum balance, deviations in the velocity profiles can be expected for the periodic hill case. Nevertheless the boundary layer profiles agree well. As in the other cases, the extended law of the wall seems to be a satisfying description for the profiles below $y^* \approx 2$.

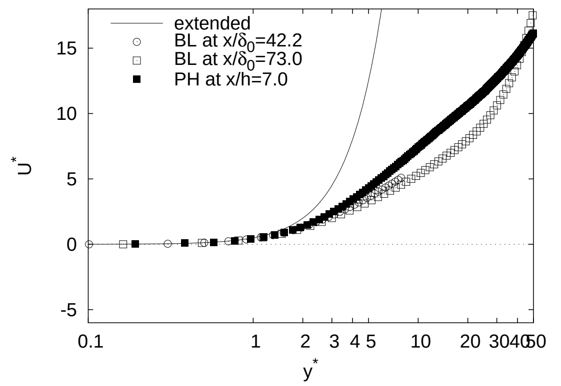

Figure 13: Velocity profiles in extended inner coordinates at $\alpha \approx 0.0$. $\tau_w \approx 0$

CONCLUSIONS

In this study, we have investigated the behaviour of terms in the differential and integrated streamwise momentum balance based on DNS of two types of separated flows. In order to be able to compare profiles from different flow situations we have used a newly proposed extended scaling (Peller et al. (2005) and Manhart et al. (2006)) which takes into account the influence of both the wall shear stress and the streamwise pressure gradient. Also taken from these works is the derivation of the extended law of the wall including the scaling parameter α. We have compared the velocity profiles to the extended law of the wall. The new extended scaling has the advantage of a smooth transition between situations dominated by wall shear stress in which the classical inner scaling is appropriate and situations dominated by streamwise pressure gradient in which the classical inner scaling fails completely. The extended scaling can be used to characterise specific flow situation. We investigate its performance in two very different flow fields, which both have been provided by highly resolved DNS. We have investigated two α values, $\alpha \approx 0.6$ and $\alpha \approx 0.0$. We have found that there is a strong agreement of the terms in the momentum balances. The assumption of a constant pressure gradient up to $y^* = 50$ is fulfilled in good agreement. Departure from the constant pressure gradient in the case of curvature effects is reflected in the profiles. Remarkable is the agreement of the amplitude of Reynolds terms and viscous terms at the maximum and thereafter. This shows that the deviations observed at the positions investigated are already due to the difference of Reynolds terms very close to the wall. The similarity of Reynolds terms, convective terms and the total stress τ_t give rise to the hope that they can be modelled. The remaining task is to quantify the present deviations and find explanations for them. Especially striking is the universal behaviour of the profiles for $\alpha = 0.6$ when the pressure gradient acts in the opposite direction compared to the wall friction. The terms in the momentum balance are identical and the velocity profile is universal till the end of the recirculation region. The performance in other flow cases with separation remains to be seen. We aim at investigating the proposed scaling also in turbulent channel flow with an adverse force field localised at the wall which artificially induces flow separation.

REFERENCES

J. Fröehlich, C. P. Mellen, W. Rodi, L. Temmerman, and M. Leschziner. Highly resolved large-eddy simulation of separated flow in a channel with streamwise periodic constrictions. *J. Fluid Mech.*, 526:19–66, 2005.

Hans-Jakob Kaltenbach. A priori testing of wall models for separated flows. *Phys. Fluids.*, 15(10):3048–3068, 2003.

M. Kalter and H.H. Fernholz. The influence of free-stream turbulence on an axisymmetric turbulent boundary layer in, and relaxing from, an adverse pressure gradient. In *5th European Turbulence Conference, Siena 1994*, 1994.

M. Manhart and R. Friedrich. DNS of a turbulent boundary layer with separation. *Int. J. Heat and Fluid Flow*, 23(5): 572–581, 2002.

M. Manhart, N. Peller, and C. Brun. A priori tests on dns of channel flow with periodic hill constrictions and dns of separating boundary layer. *Theoret. Comput. Fluid Dynamics*, (submitted), 2006.

C. P. Mellen, J. Frhlich, and W. Rodi. Large-eddy simulation of the flow over periodic hills. In *16th IMACS World Congress*, Lausanne, Switzerland, 2000.

N. Peller, C. Brun, and M. Manhart. Wall layer investigations of channel flow with periodic hill constrictions. In *DLES 6*, Poitiers, September 12.-14. 2005.

N. Peller, A. Le Duc, F. Tremblay, and M. Manhart. High-order stable interpolations for immersed boundary methods. *International Journal for Numerical Methods in Fluids*, in press, 2006.

N. Peller and M. Manhart. *Turbulent Channel Flow with Periodic Hill Constrictions*, volume 92 of *Notes on Numerical Fluid Mechanics and Multidisciplinary design.* Springer, new results in numerical and experimental fluid mechanics v edition, 2006. ISBN 3-540-33286-3.

R.L. Simpson. Turbulent boundary-layer separation. *Ann. Rev. Fluid Mech.*, 21:205–234, 1989.

M. Skote, D. Henningson, N. Hirose, Y. Matsuo, and T. Nakamura. Parallel DNS of a separating turbulent boundary layer. In *Proceedings of the Parallel CFD 2000*, Trondheim, Norway, May 22-25 2000. NTNU.

B.S. Stratford. The prediction of separation of the turbulent boundary layer. *J. Fluid Mech.*, 5:1–16, 1959.